Soils and Foundations 2015;55(4):813–828

HOSTED BY

ELSEVIER

The Japanese Geotechnical Society

Soils and Foundations

www.sciencedirect.com
journal homepage: www.elsevier.com/locate/sandf

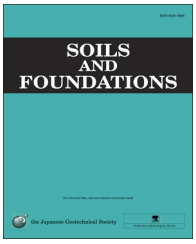

Several factors affecting seismic behaviour of embankments in dynamic centrifuge model tests

Tadao Enomoto[a,*], Tetsuya Sasaki[b]

[a]National Institute for Land and Infrastructure Management (formerly Public Works Research Institute), Tsukuba, Japan
[b]Public Works Research Institute, Tsukuba, Japan

Received 19 May 2014; received in revised form 15 December 2014; accepted 17 April 2015
Available online 21 July 2015

Abstract

A series of dynamic centrifuge model tests was conducted in order to evaluate some factors affecting the seismic performance of hillside embankments consisting of sandy or silty soils and resting on stiff base slope. The effects of seepage water elevation in embankments, toe drain, embankment height, base slope inclination, soil compaction, and fill materials on the seismic behaviour of embankments were investigated. The test results showed that: (1) the seepage water was one of the most important factors for earthquake-induced embankment failure; (2) the seismic performance of both the smaller and higher embankments was remarkably improved by installing the toe drain; (3) larger base slope inclination produced larger earthquake-induced deformation of embankments; (4) well-compacted embankments were not vulnerable to earthquake-induced damage; and (5) the seismic performance of well-compacted embankments consisting of well-graded silty soils with large fines content was higher than that of poorly graded sands under otherwise the same condition. In some tests, as observed during past strong earthquakes, delayed flow failure occurred due possibly to the multiple effects of upward seepage associated with the redistribution of excess pore water pressures generated during main shaking, continued small vibration after main shaking, and driving static shear stresses caused by the embankment weight. A series of triaxial compression and cyclic triaxial liquefaction tests was also conducted to evaluate undrained behaviour of the fill materials. The correlation between the model and laboratory element test results was presented.

keywords: Dynamic centrifuge model test; Seismic performance; Embankment; Earthquake; Seepage; Earthquake-induced delayed failure; Laboratory triaxial test

1. Introduction

During past strong earthquakes, embankments constructed on mountain/hill sides have frequently experienced catastrophic failures. A number of field investigations on geotechnical issues and case history studies based on these surveys have been carried out after the earthquakes (e.g., Public Works Research Institute (PWRI), 1971, 2008; Sasaki et al., 1994, 2012; Matsuo, 1996; Okimura et al., 1999; Koseki et al., 2006; Mori et al., 2012).

Among them, based on a number of reports on the field investigations conducted after the past earthquakes in Japan, Mori et al. (2012) summarized that the causes of damage to hillside embankments can be attributed to any of the followings; (1) the fill materials containing a high percentage of fine particles; (2) a shallow water table; (3) the loose state of fill materials due to poor compaction during the construction stages or due to the degradation of ground with time; and (4) poor treatment of the boundary between the fill and the original ground, leading a landslide type failure. As pointed out by Mori et al. (2012), the above-mentioned factor (1) tends to lead to poor compaction during the construction works. As an extreme example of the above-mentioned factor (2),

*Corresponding author.
E-mail address: enomoto-t2jz@nilim.go.jp (T. Enomoto).
Peer review under responsibility of The Japanese Geotechnical Society.

http://dx.doi.org/10.1016/j.sandf.2015.06.013

based on the measurements at the road embankments damaged severely by the 2007 Noto-Hanto earthquake, it was reported that the water table existed at the surface of the embankment toe at some sites (PWRI, 2008).

Okimura et al. (1999) performed field investigations on damage to hillside embankments during the 1995 Hyogoken-Nambu earthquake. They reported that: (1) mild original slopes smaller than about 20 degrees tended to result in the accumulation of seepage water, leading to severe damage to hillside embankments; and (2) more than 15 m high hillside embankments were damaged seriously at the top of the slope due to the amplification of seismic motion caused by their heights. PWRI (2008) also indicated that hillside embankments with 15 m or more in height tended to be vulnerable to earthquake-induced severe damage and that damage tended to be severe with decreasing ratio of inclinations near the toe to behind the embankment. These results suggest that the seismic performance of embankments is also affected by their original slope inclinations and heights.

Meanwhile, to investigate the seismic behaviour of full-scale embankments and slopes, some studies using dynamic centrifuge apparatuses have been conducted (e.g., Kutter and James, 1989; Dobry et al., 1997; Pilgrim, 1998; Okamura et al., 2001; Matsuo et al., 2002; Egawa et al., 2004; Okamura and Tamamura, 2011; Higo et al., 2012). Among them, Matsuo et al. (2002) and Higo et al. (2012) showed that the seepage water in embankments was an important factor to cause earthquake-induced damage. Matsuo et al. (2002) also showed that the soil density played an important role in controlling the occurrence of earthquake-induced failure. Dobry et al. (1997), Pilgrim (1998) and Matsuo et al. (2002) reported the effects of slope inclination on the seismic behaviour of slope. Egawa et al. (2004) and Okamura and Tamamura (2011) investigated the effects of subsoil layers on the seismic behaviour by using the embankment models on peaty soft ground and soft clay deposit, respectively. However, these experimental studies have focused on the behaviour of embankments with a height of 10 m or less in prototype scale due to limited capacities of the shaking table and soil container, in spite of damage tendency related to embankment height reported by Okimura et al. (1999) and PWRI (2008). In addition, factors affecting the seismic behaviour of hillside embankments and those mechanisms have not been systematically studied.

In view of the above, in order to evaluate the effects of several factors on the seismic performance of embankments of 15 m or more in height, a series of dynamic centrifuge model tests was conducted in the present study by using a large-scale soil container. A series of triaxial compression and cyclic triaxial liquefaction tests was also conducted to evaluate the undrained behaviour of the fill materials used for the model embankment. The correlation between the model and laboratory element test results is also presented in this paper.

2. Tested materials

Fig. 1 shows the grading curves and the laboratory compaction test data of three geomaterials used for the model and laboratory element tests. The values of specific gravity (G_s), maximum diameter (D_{max}), mean diameter (D_{50}), uniformity coefficient (U_c), fines content (F_c), natural water content (w_n), optimum water content (w_{opt}), maximum dry density (ρ_{dmax}), plasticity index (I_p) and maximum and minimum void ratios (e_{max} and e_{min}) of these materials are

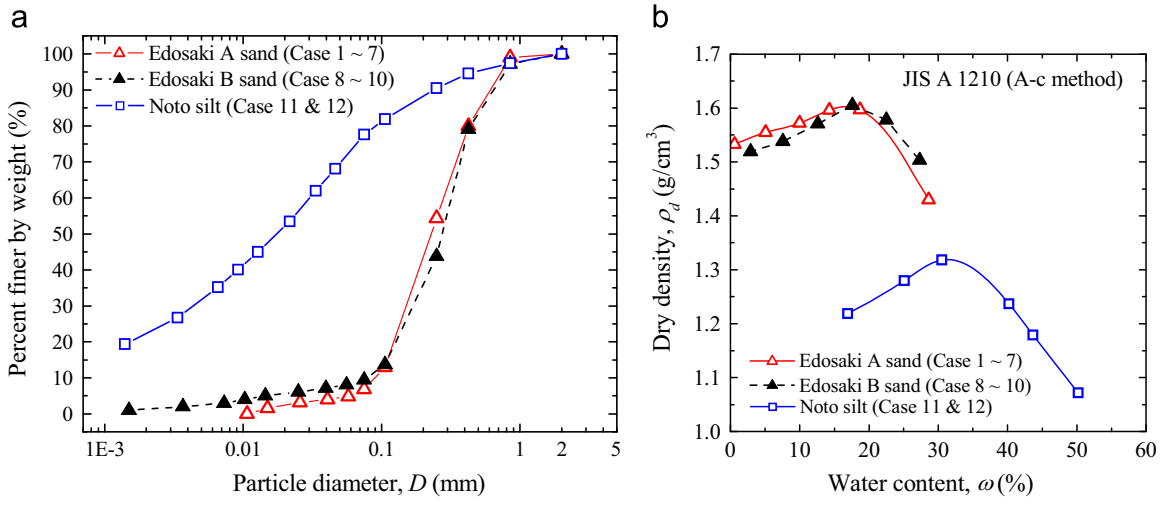

Fig. 1. Grading and compaction characteristics of geomaterials used for model and triaxial tests: (a) grading curves and (b) standard compaction test results.

Table 1
Properties of geomaterials used for model and triaxial tests.

Material	G_s	D_{max} (mm)	D_{50} (mm)	U_c	F_c (%)	ω_{opt} (%)	ω_n (%)	ρ_{dmax} (g/cm^3)	I_p (%)	e_{max}	e_{min}
Edosaki A sand	2.657	2.0	0.228	2.91	6.9	16.7	1.8	1.604	NP	1.095	0.609
Edosaki B sand	2.732	2.0	0.278	3.91	9.4	18.1	7.4	1.605	NP	-	-
Noto silt	2.696	2.0	0.0177	-[a]	77.6	31.1	39.5	1.318	29.8	-	-

[a]The value of D_{10} was not obtained.

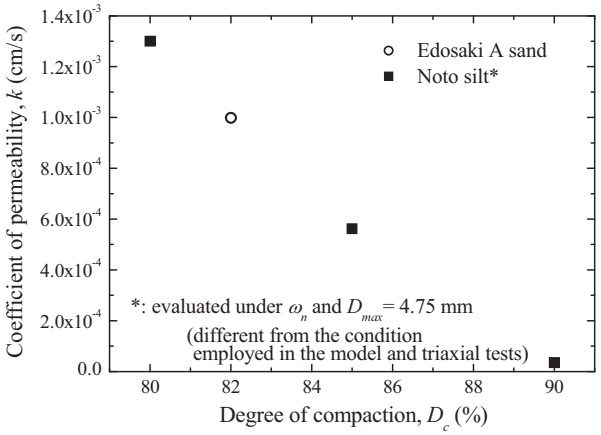

Fig. 2. Relationship between degree of compaction and coefficient of permeability.

summarized in Table 1. The values of w_{opt} and ρ_{dmax} were determined by the A-c method in Japanese Industrial Standards (JIS) A 1210, where materials were compacted in a cylindrical mold (inner diameter = 100 mm) in three layers with 25 free drops of a 2.5 kg rammer from a height of 30 cm.

Edosaki sand has been used in model testing for a long period of research at PWRI (e.g., Matsuo et al., 2002). The soil properties of Edosaki A and B sands from different batches were quite similar to each other. On the other hand, there have been few studies on centrifuge model tests using Noto silt. Noto silt was prepared by removing particles with a diameter larger than 2.0 mm from the original material which was retrieved from a road embankment damaged by the 2007 Noto-Hanto earthquake. The degree of the aggregation of soil was significant due to its large F_c value. In the present study, the degree of compaction, D_c, defined by Eq. (1) was used as a density index.

$$D_c = \rho_d / \rho_{dmax} \quad (1)$$

where ρ_d is the dry density of soil.

Fig. 2 shows the relationship between D_c and coefficient of permeability, k. In order to make sample preparation easier, the k values of Noto silt with D_{max}=4.75 mm at a w_n of about 40%, which were different from the condition employed for the model and triaxial tests as mentioned later, were evaluated by the falling head permeability tests (JIS A 1218) as a reference. However, the influence of the aggregation of soil in the specimen was significant. Therefore, these values may have been largely overestimated as compared with the condition employed for the model and triaxial tests. On the other hand, Edosaki A sand was compacted at the same water content, w_{opt}, as the model and triaxial tests for evaluating its k value in the constant head permeability test (JIS A 1218).

3. Undrained behaviour of tested soils

3.1. Test procedures

Prior to the dynamic centrifuge model tests, a series of undrained triaxial compression and undrained cyclic triaxial liquefaction tests was conducted for the materials described in the previous section. The test conditions are summarized in Table 2. As a reference, the initial relative density, D_{r0}, of specimens consisting of Edosaki A sand was also indicated in the table.

Table 2
Conditions of undrained triaxial compression and undrained cyclic triaxial liquefaction tests.

Material	Test code	Test condition	B value	ρ_{d0} (g/cm^3)	D_{c0} (%)	w_{ini} (%)	D_{r0} (%)	σ'_0(kPa)	$\sigma_d/(2\sigma'_0)$
Edosaki B sand	E1	TC	0.99	1.316	82.0	17.7	–	50	–
Edosaki A sand	E2	TC	0.97	1.365	85.1	–[a]	30.6	50	–
Edosaki A sand	E3	TC	0.98	1.457	90.8	–[a]	55.9	50	–
Edosaki B sand	E4	CTL	0.99	1.317	82.1	17.1	–	100	0.147
Edosaki B sand	E5	CTL	0.98	1.316	82.0	17.7	–	100	0.128
Edosaki B sand	E6	CTL	0.99	1.308	81.5	18.4	–	100	0.112
Edosaki B sand	E7	CTL	0.99	1.320	82.2	16.8	–	100	0.096
Edosaki A sand	E8	CTL	1.00	1.367	85.2	–[a]	31.2	100	0.147
Edosaki A sand	E9	CTL	0.97	1.368	85.3	–[a]	31.5	100	0.128
Edosaki A sand	E10	CTL	1.00	1.361	84.9	–[a]	29.5	100	0.138
Edosaki A sand	E11	CTL	0.97	1.366	85.2	–[a]	30.9	100	0.164
Edosaki A sand	E12	CTL	0.98	1.448	90.3	–[a]	53.6	100	0.194
Edosaki A sand	E13	CTL	0.98	1.457	90.8	–[a]	55.9	100	0.175
Edosaki A sand	E14	CTL	0.98	1.460	91.0	–[a]	56.7	100	0.157
Edosaki A sand	E15	CTL	0.98	1.455	90.7	–[a]	55.4	100	0.168
Noto silt	N1	TC	0.95	1.082	82.1	23.2	–	50	–
Noto silt	N2	CTL	0.98	1.087	82.5	22.3	–	50	0.199
Noto silt	N3	CTL	0.99	1.080	81.9	22.6	–	50	0.149
Noto silt	N4	CTL	0.98	1.078	81.8	22.9	–	50	0.176
Noto silt	N5	CTL	0.99	1.082	82.1	22.6	–	50	0.234
Noto silt	N6	CTL	1.00	1.085	82.3	22.5	–	50	0.190

TC: Undrained triaxial compression test, CTL: Undrained cyclic triaxial liquefaction test.

[a]The target value was w_{opt} (=16.7%), however, the detailed measured data was unavailable.

Small-scale cylindrical specimens having a dimension of 5 cm in diameter and 10 cm in height were produced by compacting wet materials inside a split mold in five layers using a hammer to the prescribed initial degree of compaction, D_{c0}, under the prescribed initial water content, w_{ini}. The specimen was set into the triaxial apparatus and was made saturated under the isotropic state of an effective mean principal stress $p' = (\sigma'_v + 2\sigma'_h)/3 = 20$ kPa, where σ'_v and σ'_h are the effective vertical and horizontal principal stresses, respectively. After isotropic compression was performed toward the target initial effective confining stresses, σ'_0, shown

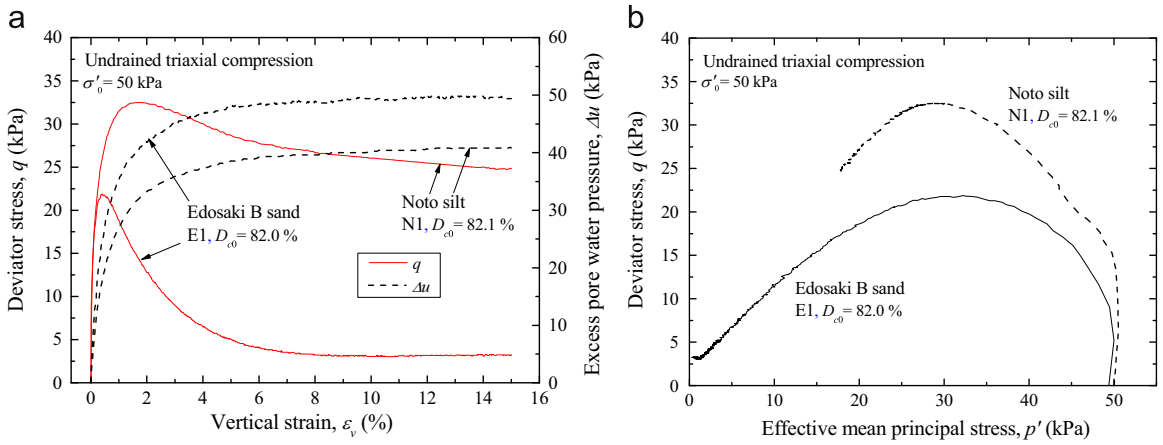

Fig. 3. Results from undrained triaxial compression tests on Edosaki B sand and Noto silt with D_{c0}=82%: (a) q-ε_v-Δu relations and (b) effective stress paths.

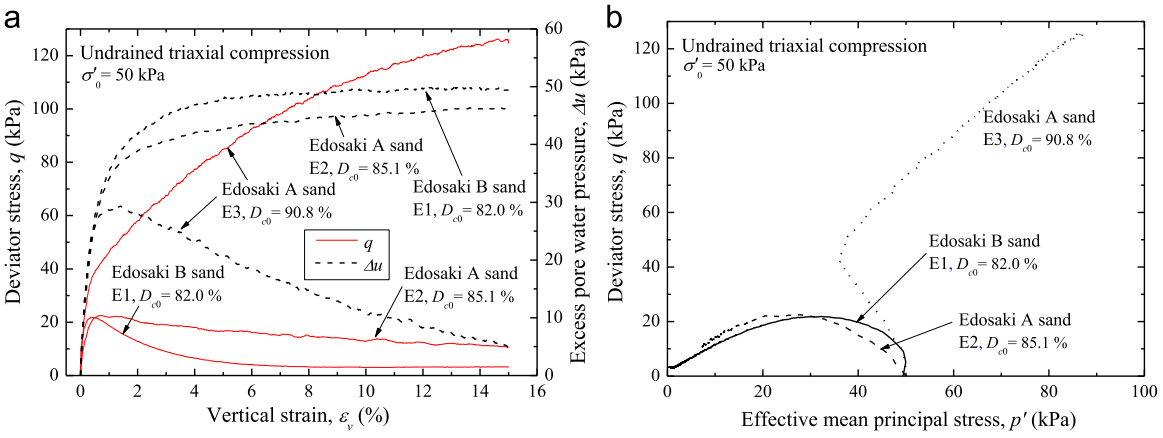

Fig. 4. Results from undrained triaxial compression tests on Edosaki sand with different D_{c0} values: (a) q-ε_v-Δu relations and (b) effective stress paths.

in Table 2, strain-controlled vertical monotonic loading or stress-controlled vertical cyclic loading was applied at a constant vertical strain rate $\dot{\varepsilon}_v$=0.1%/min or a constant frequency f=0.1 Hz, respectively, under undrained conditions. The deviator stress, $q=\sigma'_v-\sigma'_h$, and vertical strain, ε_v, were evaluated based on the measurements with a load cell placed inside the triaxial cell and an external displacement transducer, respectively.

3.2. Results of monotonic shear tests

Fig. 3 shows the results from undrained triaxial compression tests on Edosaki B sand and Noto silt with D_{c0}=82% conducted under σ'_0=50 kPa. The specimen consisting of poorly graded Edosaki B sand with F_c=9.4% exhibited a peak strength at a relatively small strain level and subsequently showed a significant drop in q over a wide range of ε_v, leading to static liquefaction (Castro, 1969). On the other hand, the specimen consisting of well-graded Noto silt with F_c=77.6% exhibited larger peak and residual strengths. Correspondingly, the excess pore water pressure, Δu, of test E1 was larger than that of test N1.

Fig. 4 shows the effects of D_{c0} on the undrained behaviour of Edosaki sand obtained from three triaxial compression tests conducted under σ'_0=50 kPa. The difference between peak strengths of tests E1 and E2 was small while the residual strength of the latter case with D_{c0}=85% was much larger than that of the former one with D_{c0}=82%. Correspondingly, the difference between Δu of these two tests was very small in the pre-peak regime while it was obvious in the post-peak one. The reason for the significant difference in the post-peak behaviour against the small variation in D_{c0} is not well understood, so further investigations may be required to clarify this issue. On the other hand, the specimen with D_{c0}=90% exhibited dilative behaviour without the peak strength unlike those with D_{c0}=82 and 85%.

3.3. Results of liquefaction tests

Fig. 5 shows the comparison of the results from two undrained cyclic triaxial liquefaction tests on Edosaki B sand and Noto silt which were conducted under very similar cyclic stress ratios, $\sigma_d/(2\sigma'_0)$, where σ_d denotes the single amplitude cyclic vertical stress. The excess pore water pressure ratio, R_u, was evaluated by

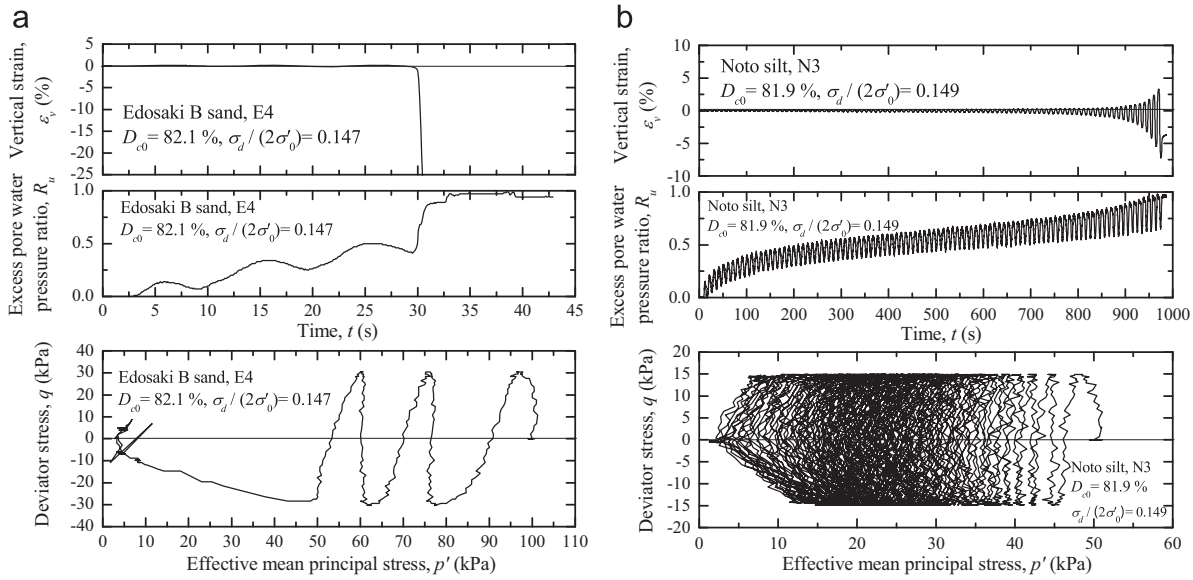

Fig. 5. Comparison of time histories of vertical strain and excess pore water pressure ratio, and effective stress paths obtained from two undrained cyclic triaxial liquefaction tests on: (a) Edosaki B sand and (b) Noto silt.

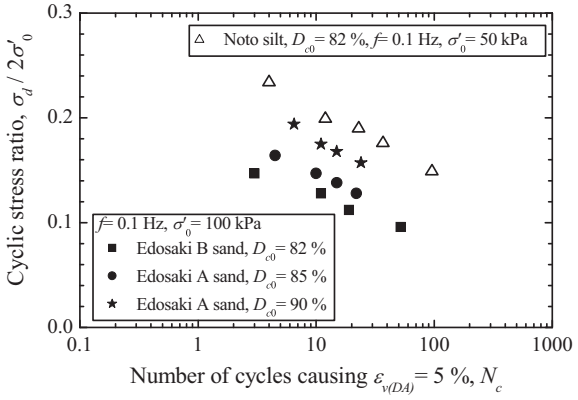

Fig. 6. Relationship between cyclic stress ratio and number of cycles to cause double amplitude vertical strain of 5%.

Eq. (2).

$$R_u = \Delta u/\sigma'_0 \tag{2}$$

As seen from the time histories of ε_v and R_u, deformation of both specimens consisting of Edosaki B sand and Noto silt, respectively, suddenly increased when R_u exceeded about 0.6. Under a condition of D_{c0}=82%, the behaviours of the specimens consisting of Edosaki B sand and Noto silt were similar to those of loose clean and dense sands in laboratory liquefaction tests, respectively.

Fig. 6 shows the relationship between $\sigma_d/(2\sigma'_0)$ and the number of cycles to cause double amplitude vertical strain $\varepsilon_{v(DA)}$ of 5%, N_c. Under a condition of D_{c0}=82%, it can be seen that the liquefaction resistance, R_L, which is the cyclic stress ratio defined at N_c=15, of Noto silt with F_c=77.6% was about 70% larger than that of Edosaki B sand with F_c=9.4%. It was also observed that the R_L value of Edosaki sand increased with increasing D_{c0}. However, the R_L value of Noto silt with D_{c0}=82% was still larger than that of Edosaki A sand with D_{c0}=90%.

Regarding the effects of fines content on soil liquefaction, some studies showed that fine particles in specimens increased the liquefaction resistance while others reported the opposite results. Among them, Chien et al. (2002) reported that, under constant relative density, the liquefaction resistance of silty sands with the F_c values ranging from 0 to 30% decreased with increasing fines content. On the other hand, as pointed out by Law and Ling (1992) and Sitharam et al. (2013), the liquefaction resistance of silty sands initially decreased with increasing fines content under constant void ratio, however, it increased when exceeding a certain F_c value. A similar trend for silty sands under constant relative density with F_c values ranging from 0 to 40% or more was reported by Hwang et al. (1993) and Arab and Belkhatir (2012). In addition, it has been shown that the plasticity of soils also affected their liquefaction resistances (e.g., Ishihara and Koseki, 1989; Law and Ling, 1992; Park and Kim, 2013). Among them, Ishihara and Koseki (1989) reported that the liquefaction resistance increased with increasing I_p. However, since the amount of data in the present study were too small, it was difficult to derive any general trend in terms of the effects of fines content and plasticity on soil liquefaction under constant D_c value. Further investigations should be carried out to clarify this.

Although soil properties are known to be affected by the confining stress levels, a limited number of studies have been conducted on their effects on the liquefaction properties of soils. Among them, based on results from undrained cyclic triaxial tests, it was pointed out that the liquefaction resistance of clean sands increased with the decrease in the confining stress levels (e.g., Mochizuki and Fukushima, 1993; Kanatani et al., 1994; Amaya et al., 1997; Hyodo et al., 2002). According to these studies, however, the difference among the liquefaction resistances of medium dense sands at σ'_0 ranging from 50 to 100 kPa was small. Although the levels of σ'_0 employed in the liquefaction tests were

Table 3
Scale factors in dynamic centrifuge model tests.

Scale	Acceleration	Density	Length	Mass	Force	Stress	Strain	Time		Viscosity
								Dynamic	Seepage	
Prototype	1	1	1	1	1	1	1	1	1	1
Model	N	1	1/N	$1/N^3$	$1/N^2$	1	1	1/N	$1/N^2$	1/N

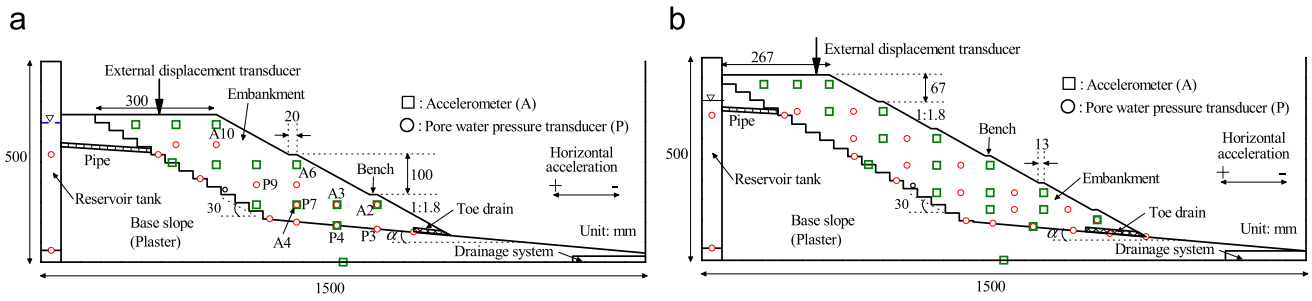

Fig. 7. Typical cross-sections of test models: (a) cases 1 through 7 and 10 through 12, and (b) cases 8 and 9.

Table 4
Conditions of dynamic centrifuge model tests.

Case	Centrifugal acceleration (g)	H (cm)[a]	H (m)[b]	Fill material	a (degrees)	D_{c0} (%)	w_{ini} (%)	Toe drain		h_w (m)[b]
								Length(m)[b]	Material[c]	
1	50	30	15	Edosaki A sand	5	82.5	16.7	2.5	No. 4	2.83
2	50	30	15	Edosaki A sand	5	82.2	16.7	9	No. 4	2.61
3	50	30	15	Edosaki A sand	5	82.4	16.7	14.5	No. 4	0.70
4	50	30	15	Edosaki A sand	5	82.0	16.7	14.5	No. 3	0.00
5	50	30	15	Edosaki A sand	5	85.4	16.7	2.5	No. 3	2.89
6	50	30	15	Edosaki A sand	0	89.9	16.7	0	–	4.03
7	50	30	15	Edosaki A sand	0	85.7	16.7	4.5	No. 3	3.94
8	75	40	30	Edosaki B sand	5	81.5	15.3	21.75	No. 3	0.00
9	75	40	30	Edosaki B sand	5	82.2	15.3	11.25	No. 3	0.98
10	50	30	15	Edosaki B sand	5	82.2	15.3	2.5	No. 4	4.21
11	50	30	15	Noto silt	5	82.6	40.3	4.5	No. 3	0.53
12	50	30	15	Noto silt	5	82.0	25.8	2.5	No. 3	2.94

[a]In model scale.
[b]In prototype scale.
[c]Silica sand (the k values of silica sands No. 3 and 4 were approximately 400 and 50 times larger than those of Edosaki sand respectively when roughly estimated by the method proposed by Creager et al. (1945)).

different for each material in the present study, the effects on the results can be considered as insignificant.

4. Procedures of model tests

A series of model tests was conducted by using a dynamic centrifuge apparatus with an effective radius of 6.6 m at PWRI (Matsuo et al., 1998). Scale factors for acceleration, density, length, mass, force, stress, strain, time and viscosity in dynamic centrifuge model tests are shown in Table 3.

In order to simulate the seismic behaviour of hillside embankments, the models were constructed on the stiff base slope made from plaster in a soil container. After having applied centrifugal accelerations to the models, a fluid was introduced into the model embankments. When the pore water pressures reached target values and global steady state condition was achieved, the model was horizontally shaken. Details of the test procedures are presented below.

Typical cross-sections of the models are shown in Fig. 7. The test condition for each model is summarized in Table 4. The models were prepared in a large-scale rigid container, 1.5 m long, 0.3 m wide and 0.5 m high, with both sides made of high-strength glass for observation. The stiff base slope consisting of two different inclinations, 30 and α degrees, was made from plaster. As shown in Table 4, 0 or 5 degrees was employed as α. Sand paper was glued to the surface of the base slope to ensure mechanical friction at the interface between the plaster slope and sand particles. In order to provide the seepage water into the embankments, as

shown in Fig. 7, a reservoir tank and a pipe were installed at the end of the rigid container and in the base slope, respectively.

The model embankment with side slopes of 1:1.8 was made carefully by compacting fill materials by means of a wooden plate at the respective w_{ini} values shown in Table 4. The w_{opt} value was employed in cases 1 through 7 as w_{ini}, while the model embankments of cases 8 and 9 were made at the water content which was slightly drier than w_{opt} to avoid their failures possibly caused by the large applied centrifugal acceleration and their heights. Noto silt was compacted under around w_n in case 11, however, the influence of the aggregation of soil in the model embankment was significant. An attempt was made to restrict its effect in case 12, reducing the w_{ini} value by about 15%. Since the peak internal friction angle and secant modulus of a similar fine sandy soil (Inagi sand) obtained from drained plane strain compression tests were rather independent of the water content at compaction as confirmed by Tatsuoka (2011), it was assumed in the present study that the effects of different w_{ini} on the seismic performance of embankments were insignificant. Filling and compaction were repeated in 12 layers of 25 and 33 mm elevations each for the models shown in Fig. 7(a) and (b), respectively. During model construction, accelerometers (A) and pore water pressure transducers (P) were embedded at prescribed locations shown in Fig. 7. In addition, mesh lines made of white-colored silica sand No.7 were placed at the side of the embankment to visually observe the model deformation through a transparent glass plate.

After model construction, the models shown in Fig. 7(a) and (b) were spun up to centrifugal accelerations of 50g and 75g, respectively. A fluid, methyl-cellulose solution, which was 50 or 75 times more viscous than water, was then introduced into the reservoir tank through the rotary joint of the centrifuge apparatus, while the discharge rate was carefully controlled. Only in case 12, water was used as the pore fluid in order to make it easy to induce the rise in the seepage elevation, due to the low permeability of Noto silt, although the similitude law was not satisfied. Since the k value of Noto silt was deemed to be much smaller than that of Edosaki sand as mentioned previously, it can be assumed that the order of the dissipation rate of Δu generated during shaking in case 12 was almost equal to or even smaller than any of the test cases using Edosaki sand.

Through the process of seepage, elevation of the phreatic line was monitored based on the measurements with the pore water pressure transducers embedded in the model and images from a high speed camera fixed on the centrifuge apparatus. When the pore water pressures reached target values and global steady state condition, the model was horizontally shaken. In some tests, however, the pore water pressures did not reach the steady states locally. As shown in Fig. 8, the ground motion recorded at the Kobe Maritime Observatory during the 1995 Hyogoken-Nambu earthquake was used as the input acceleration for the model shown in Fig. 7(a). Due to a limited excitation capacity of the shaking table under the higher centrifugal acceleration, the same input could not be employed for the model shown in Fig. 7(b). The ground motion recorded at the Shichihou bridge during the 1993 Hokkaido-Nanseioki earthquake was inputted for the latter model. The settlement at the crest or the top of the slope, S or S', respectively, was measured with an external displacement transducer throughout the tests.

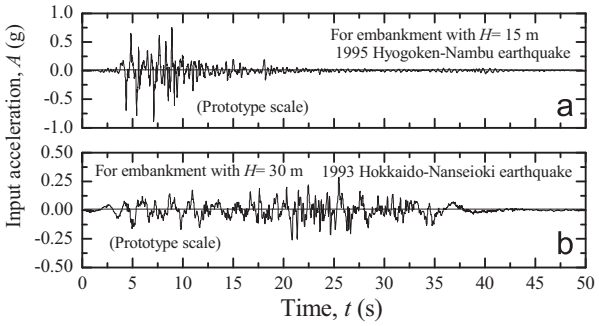

Fig. 8. Typical input accelerations in prototype scale for: (a) cases 1 through 7 and 10 through 12, and (b) cases 8 and 9.

In shaking table tests using rigid soil containers, when a soil layer is prepared along the side walls, shear deformation of ground during shaking can be constrained to some extent near the wall which is perpendicular to the shaking direction. In the present study, however, since the model embankments were constructed far from the rigid side walls in the shaking direction, it was assumed that the effect of the boundary on the seismic behaviour was insignificant. Furthermore, as mentioned later, since collapsed soils from model embankments did not reach the wall which was perpendicular to the shaking direction, very little if any impact energy was generated at the boundary.

5. Model test results and discussions

The test results shown in the following sections are represented in the prototype scale, unless otherwise mentioned. The definition of the acceleration direction is described in Fig. 7. Excluding the time history data of the embankment settlement, the residual value of S evaluated from photographs taken after shaking was used in the following analyses, due to the limited measurement capacity of an external displacement transducer (possible measurement range and resolution in the model scale = 0–50 mm and 0.1 mm, respectively).

The earthquake-induced deformations of embankments, which were sketched after shaking, together with phreatic lines for the respective test cases are shown in Fig. 9. As typically shown in the figure, it was confirmed throughout the test that the mass of collapsed soils which flowed out from the model embankments did not reach the rigid side wall which was perpendicular to the shaking direction. This suggests that the effect of the boundary condition on the seismic behaviour was insignificant.

5.1. Effects of seepage water and toe drain

The models in cases 4 and 10 had an embankment height (in prototype scale), H, of 15 m and consisted of Edosaki A and B sands, respectively, with $D_{c0}=82\%$ while their water tables were largely different as shown in Fig. 9. The water tables near the crest and embankment toe were shallow and deep, respectively, in case 4 while they were opposite in case 10.

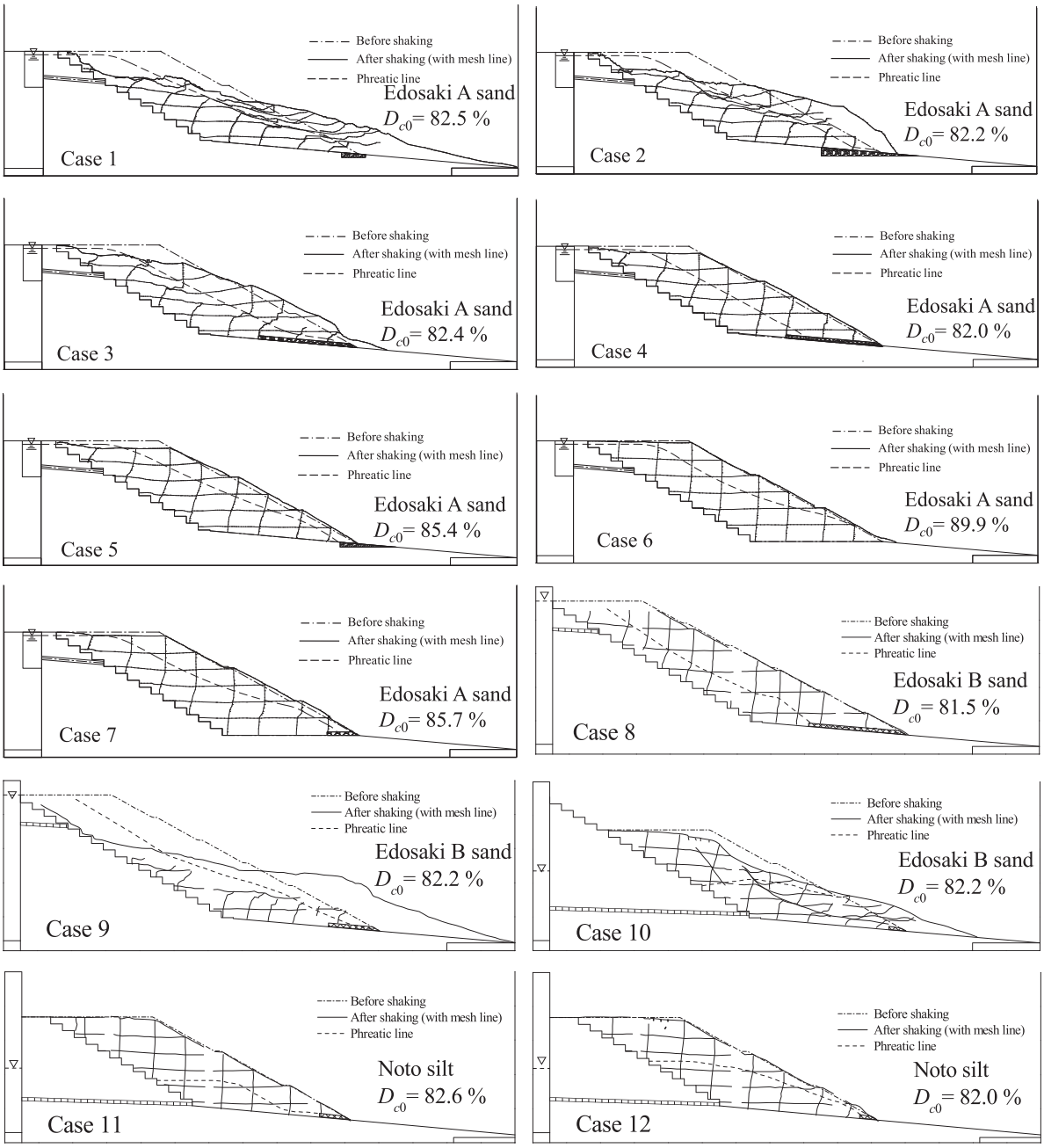

Fig. 9. Observed deformations of model embankments after shaking.

The earthquake-induced deformation in case 4 was relatively small. In such a case, the restoration work of the embankment can be conducted easily for a short period of time. On the contrary, severe landslide-like damage occurred in case 10 due to a progressive failure of the embankment toe inducing damage to the crest. This difference may have been attributed to the different water tables, suggesting that the effect of seepage water in the toe on the seismic performance of embankments may be more significant than that near the top of the slope. To represent the effects of the water table near the toe on the seismic performance of embankments, the seepage water elevation measured from the plaster surface at the first bench, h_w, is used as an index in the following discussions. The definition of h_w is schematically shown in Fig. 10.

Fig. 10 shows the relationship between S and h_w obtained from five tests on models having $H=15$ m and consisting of Edosaki A sand with $D_{c0}=82\%$. It was shown in Fig. 9 that the seepage water elevations of cases 1 through 4 were similar near the crest since a pipe to provide the seepage water was installed at the same position near the top of the base slope. On the other hand, the seepage water elevations were lowered near the embankment toe with increasing length of drain. As seen from Fig. 10, the value of S increased remarkably with increasing h_w, which strongly suggests that the seepage water in embankments is one of the most important factors for earthquake-induced failure. This trend of behaviour is consistent with the test results reported by Matsuo et al. (2002) and Higo et al. (2012), and one of the causes of damage to hillside embankments summarized by Mori et al.

(2012) which was described earlier. In particular, the S value of case 4 was about 75% smaller than that of case 1, indicating that the effects of seepage water in the toe on the seismic performance of embankments were rather significant.

In Fig. 10, the result from test case 5 with $D_{c0}=85\%$ is also plotted. The S value of case 5 was much smaller than that of case 1 in spite of their similar levels of h_w. The detailed analyses of the effects of the embankment density will be described later.

Fig. 11(a) shows the relationship between the pore water pressure, u, measured with P3 and the elapsed seepage time, t_s, for cases 1 through 4. The value of u did not reach the steady state at P3 in some tests. In the figure, the length of toe drain, l, and its material for each test case are indicated. When compared at the same t_s, the value of u tended to decrease with increasing l. In particular, in cases 3 and 4, the values of u remained zero during a certain time range of seepage before which they started to increase at smaller rates than those of cases 1 and 2 after exceeding the capacities of toe drains. The difference between cases 3 and 4 was attributed to the permeabilities of drain materials, where the k values of silica sands Nos. 3 and 4 were approximately 400 and 50 times larger than those of Edosaki sand respectively when roughly estimated by the method proposed by Creager et al. (1945) (see the annotation in Table 4). Consequently, the seismic performance of embankments was enhanced with an increase in the value of l as shown in Fig. 11(b). Higo et al. (2012) also showed that the seepage water elevation in the embankment was lowered by installing a toe drain in dynamic centrifuge model tests.

In fact, Sasaki et al. (2012) reported that the installation of a gravel toe drain at the foot of the levee slope was successful in lowering the water level at the time of the 2011 off the Pacific coast of Tohoku earthquake as well and consequently reducing seismic damage.

5.2. Delayed failure

Fig. 12 shows the time history of S for cases 1 through 4 which are discussed in the above section. Fig. 13 shows the photographs of deformed embankments of these four cases taken by a high speed camera at two selected elapsed times of shaking. Fig. 14 compares the distributions of R_u for these four tests at two selected elapsed times of shaking, where R_u is obtained by replacing σ'_0 with the initial vertical effective stress, σ'_{v0}, in Eq. (2). The σ'_{v0} value was roughly estimated at each location by using Eq. (3).

$$\sigma'_{v0}=\rho_t g z \quad (0\le z\le z_1)$$
$$\sigma'_{v0}=\rho_t g z_1+\rho' g(z-z_1) \quad (z_1<z\le z_2) \tag{3}$$

where ρ_t and ρ' are the total and submerged densities of the embankment, respectively; g is the gravity acceleration; and z, z_1 and z_2 are the depth from the embankment surface, and

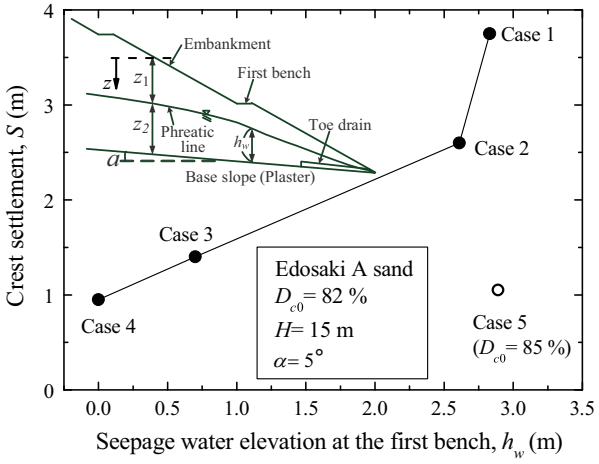

Fig. 10. Effects of seepage water elevation on crest settlement of embankments having a height of 15 m.

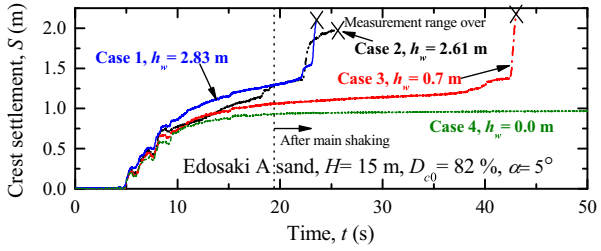

Fig. 12. Time history of crest settlement of 15 m high embankments with different water tables.

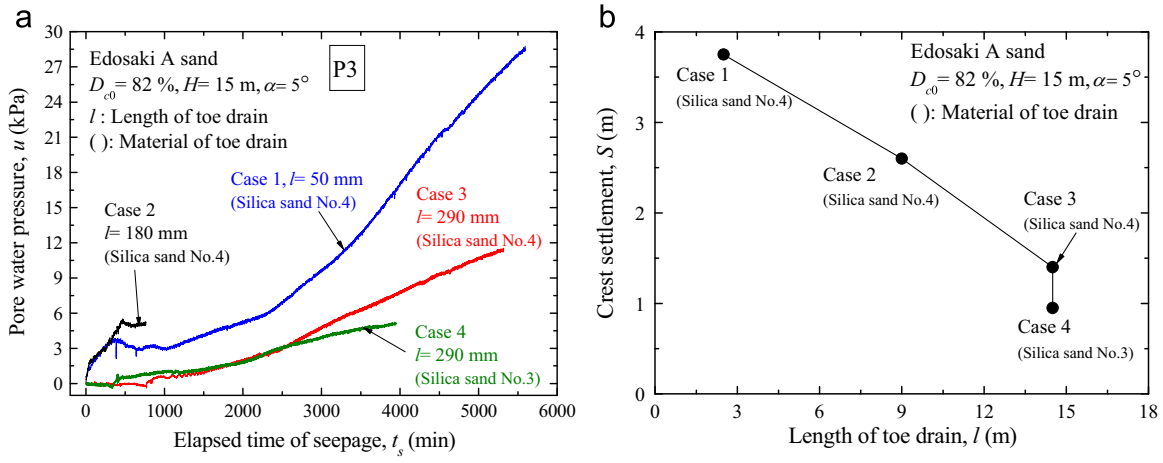

Fig. 11. Effects of toe drain on: (a) time history of pore water pressure measured with P3 during process of seepage and (b) crest settlement.

thicknesses of the unsaturated and saturated embankment layers, respectively, as schematically shown in Fig. 10. Fig. 15 shows the difference among response accelerations, A_{res}, recorded by A6 for these four tests. The following trends were observed from Figs. 12 through 15.

1) In cases 1 through 3, the amount of S after the main shaking has ceased was larger than that developed during the main shaking. In addition, after the end of the main shaking, the settlement rate, $\dot{S}$, increased suddenly at the elapsed times of shaking, t, of about 22 s in cases 1 and 2 and about 42 s in case 3, resulting in the delayed failure. On the other hand, the deformation of case 4 stopped as soon as the main shaking ended.
2) Immediately after the main shaking, deformation was concentrated below the water table and near the embankment toe. On the other hand, the above-mentioned delayed failure occurred near the water table.
3) Complete liquefaction did not occur during the main shaking although some data may be unreliable due to the malfunctioning

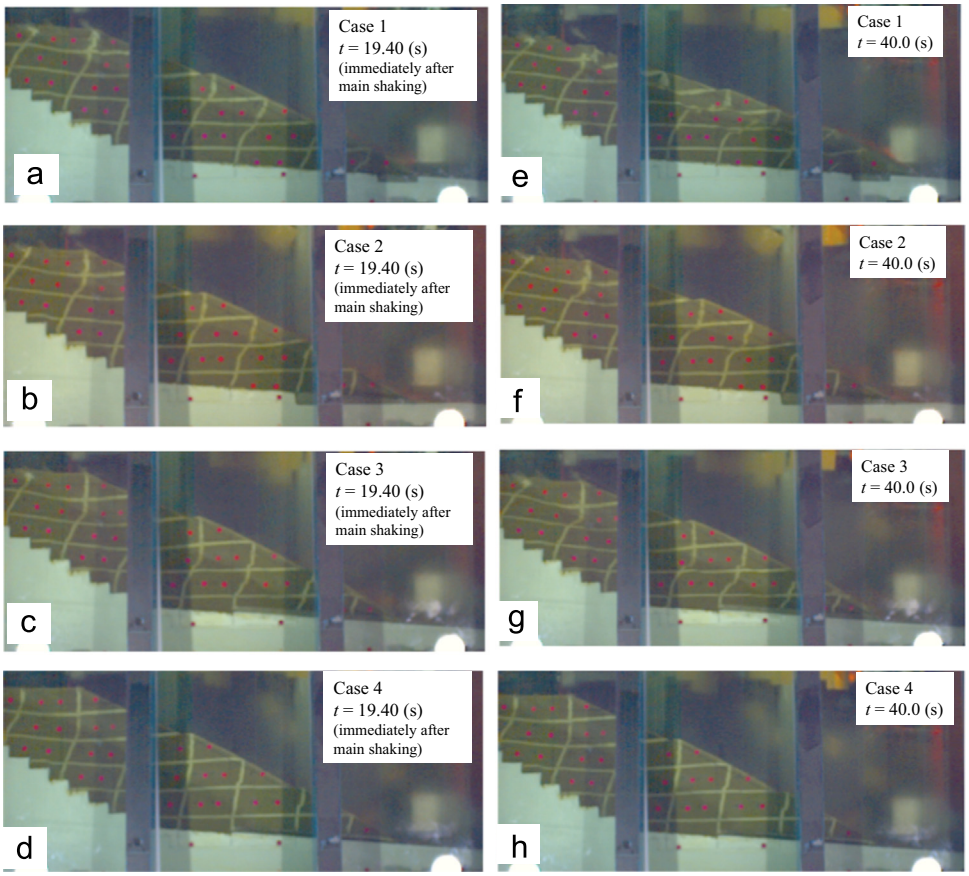

Fig. 13. Photographs of deformed model embankments taken by a high speed camera at two selected elapsed times of shaking: (a) through (d) at t=19.40 (s) (immediately after main shaking), and (e) through (h) at t=40.0 (s).

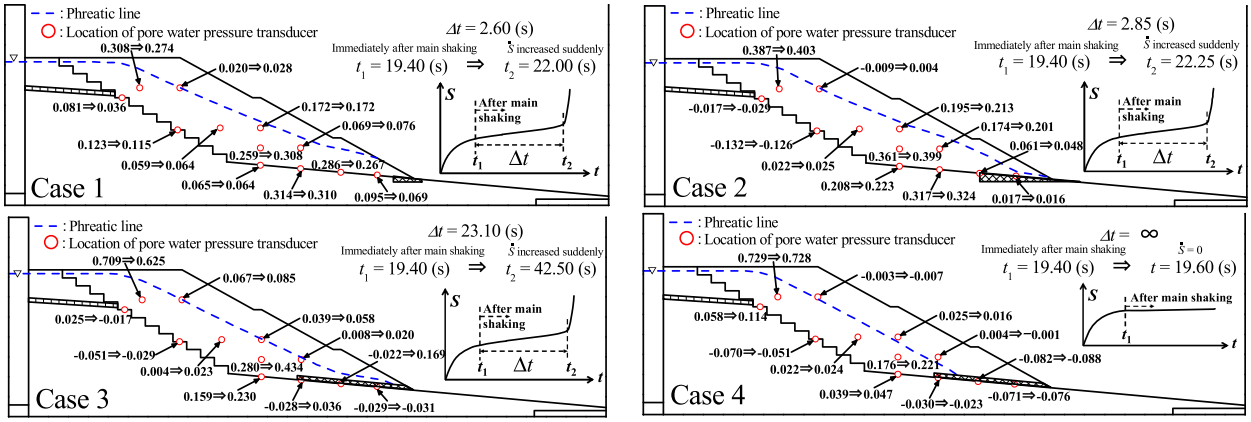

Fig. 14. Change in distribution of excess pore water pressure ratio after main shaking in cases 1 through 4.

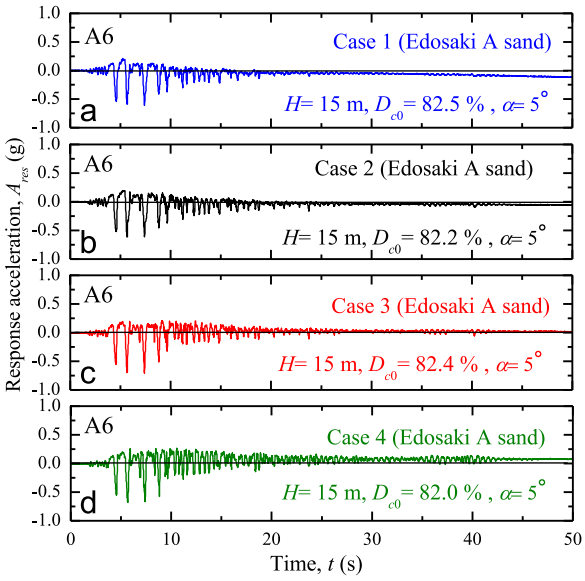

Fig. 15. Time history of response accelerations of 15 m high embankments with different water tables.

of some pore water pressure transducers. It was confirmed that complete liquefaction also did not occur even after the main shaking. The average shear stress ratio, $(\tau/\sigma'_{v0})_{ave}$, in the negative acceleration direction at A4 during the main shaking, which was roughly estimated by Eq. (4), was about 0.1 for cases 1 through 4. In cases 1 through 3, when compared with the result of triaxial test E7 conducted under a similar condition, the R_u value from P7, which was located at the same elevation as A4, immediately after the main shaking was approximately consistent with the laboratory result at the number of cycles of 15 (i.e., $R_u \fallingdotseq 0.3$).

$$(\tau/\sigma'_{v0})_{ave} = \int_0^{t_1} [\rho \cdot z \cdot A_{res}(t) \cdot g]dt/(\sigma'_{v0} \cdot t_1) = \int_0^{t_1} A_{res}(t)dt/t_1 \quad (4)$$

where ρ is the soil density of the embankment; and t_1 is the time immediately after the main shaking.

4) From Fig. 14, there was a slight trend of upward seepage associated with the redistribution of Δu generated during the main shaking in cases 1 through 3. However, in general, the amount of the redistribution was not so large.
5) The amplitude of A_{res} during shaking tended to become smaller in order of cases 1, 2, 3 and 4. This behaviour may be due to: (a) the reduction in the shear modulus of embankments caused by the accumulation of Δu; and (b) earthquake-induced deformation below the water table.

It was reported by Seed (1979) that the San Fernando Dam also collapsed several seconds after the shaking stopped. He suggested that the time delay was caused by pore water flowing from zones of high pore pressure to the zone of potential failure (i.e., redistribution of excess pore water pressures generated during shaking). Similarly, during the 1964 Niigata earthquake and the 1983 Nihonkai-Chubu earthquake, deformation continued to occur progressively due to liquefaction after the earthquake motion terminated (Kawakami and Asada, 1966; Hamada, 1992a, b). In the 1964 Niigata earthquake, after the earthquake motion terminated, an apartment house in Kawagishi-Cho continued to settle and tilt for a few minutes (Kawakami and Asada, 1966) and a girder of the Showa Bridge fell down after a few minutes (Japanese Society of Civil Engineers, 1966). Based on the dynamic centrifuge model test results, Okamura et al. (2001) assumed that weak aftershock or continuous vibration after the main shock acting at the already liquefied sand layer was the main cause of the continuous ground deformation. Sento et al. (2004) studied another mechanism of the delayed failure which was attributed to shearing due to upward seepage associated with the redistribution of excess pore water pressures generated during shaking. They revealed that, in the case of a heterogeneous multi-layered inclined ground, residual ground deformation developed after shaking was concentrated at the layer immediately below the low-permeability one due to the trapped pore water, while no residual displacement occurred when the coefficient of permeability was similar in every layer.

Some dynamic centrifuge model tests have been conducted to investigate post-liquefaction lateral spreading problem (e.g., Dobry et al., 1997; Okamura et al., 2001). In most tests, however, flow deformation ceased as soon as the shaking ended. It may be possible that this behaviour was the result of the use of homogeneous grounds consisting of clean sands. On the other hand, a similar delayed failure of a clay embankment was reported by Kutter and James (1989). In their centrifuge model tests, two pore water pressure transducers located at both sides of the failure surface showed drastic changes when the delayed failure occurred, suggesting an evidence of redistribution of excess pore water pressures generated during shaking.

The reason for the delayed failure observed in the present study can be explained as follows. In cases 1 through 4, homogeneous embankments were prepared using Edosaki A sand with $Fc = 6.9\%$, but it should be noted that these models had a boundary between the saturated and unsaturated embankment layers due to the seepage water. Since the k values of saturated fine sands are higher than those of unsaturated ones, this boundary may have played a role as a low-permeability layer, which may have led to residual deformation at the water table after the main shaking due to the trapped pore water. In addition, continuous deformation can be caused by continuous small amplitude vibration after the main shaking as revealed by Okamura et al. (2001). In their centrifuge model tests, lateral displacement of slightly sloping ground occurred due to the low amplitude shaking of $0.04g$ applied to the already liquefied soil after the main shock. Taking into account the fact that complete liquefaction did not occur in cases 1 through 3, however, another cause of the delayed failure can be considered. After the main shaking, the decreased strength of Edosaki A sand could not sustain the downslope driving force caused by the embankment weight due possibly to the accumulation of Δu, which may have led to the delayed failure due to the undrained sustained loading. The sudden increase in S after the main shaking, which caused the

delayed failure, may have been attributed to the multiple effects of the three possible reasons cited above.

Kutter and James (1989) pointed out that the magnitude of the time delay depended on many factors, including soil permeability, coefficient of consolidation and embankment geometry. Sento et al. (2004) also reported that the duration and magnitude of flow deformation are governed by the thickness of liquefaction layer beneath the low-permeability one as well as by the ground permeability. The test results shown in Fig. 16 suggest that, with decreasing h_w (i.e., the thickness of saturated layer at the first bench which may be liquefible), the time delay schematically defined in Fig. 14, Δt, increased while the crest settlement developed after the end of the main shaking, ΔS, decreased.

5.3. Effects of seepage water in higher embankment

Fig. 17 shows the relationship between S and h_w obtained from two tests on models having $H=30$ m and consisting of Edosaki B sand with $D_{c0}=82\%$. As shown in Fig. 9, the seepage water elevations of cases 8 and 9 were very similar at the top of the slope while their differences became large near the embankment toe due to the different lengths of the drain. As seen from the comparison between the data of cases 8 and 9 in Fig. 17, the seismic performance was improved remarkably by lowering the seepage water elevation in the embankment toe. This observation also suggests that the effects of seepage water in the embankment toe were more significant than those near the top of the slope.

Fig. 18 shows the time history of S' for cases 8 and 9. In case 8, the amount of S' after the main shaking has ceased was the same as that developed during the main shaking, while continuous deformation occurred in case 9, leading to delayed failure. Fig. 19 compares the distributions of R_u for case 9 at two selected elapsed times of shaking. Complete liquefaction did not occur throughout the test. Some data in Fig. 19 appears to show slight trend of upward seepage associated with the redistribution of Δu generated during the main shaking, as seen in cases 1 through 3. However, the amount of the redistribution was not so large.

5.4. Effects of base slope inclination

Fig. 20 shows the relationship between S and α obtained from two model tests on Edosaki A sand with $D_{c0}=85\%$, where those embankment models with $H=15$ m had similar water elevations as shown in Fig. 9. The residual displacement of case 5 with $\alpha=5$ degrees was much larger than that of case 7 with a horizontal base slope, due to the increase in the downslope driving force caused by the embankment weight. A similar test result on the infinite slope model was reported by Matsuo et al. (2002).

5.5. Effects of soil compaction

Fig. 21 shows the relationship between S and D_{c0} obtained from four model tests on Edosaki A sand with different densities, where those embankment models with $H=15$ m had similar water elevations as shown in Fig. 9. The value of S decreased obviously with an increase in D_{c0}. This result suggests that well-compacted embankment is not vulnerable to earthquake-induced damage for the motions considered in this study. This trend is consistent with the test results reported by Matsuo et al. (2002). As shown in Fig. 20, the effects of

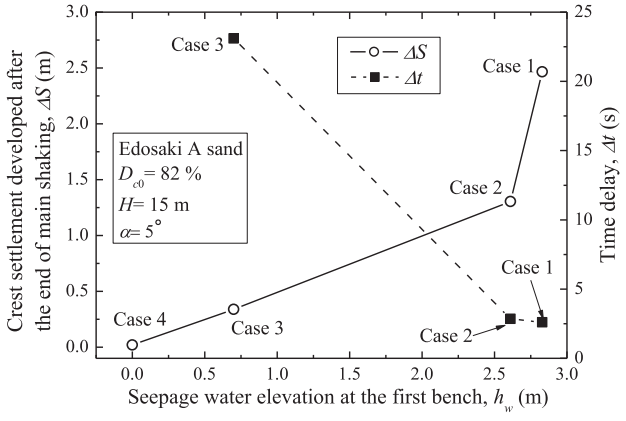

Fig. 16. Effects of seepage water elevation on time delay and magnitude of flow deformation.

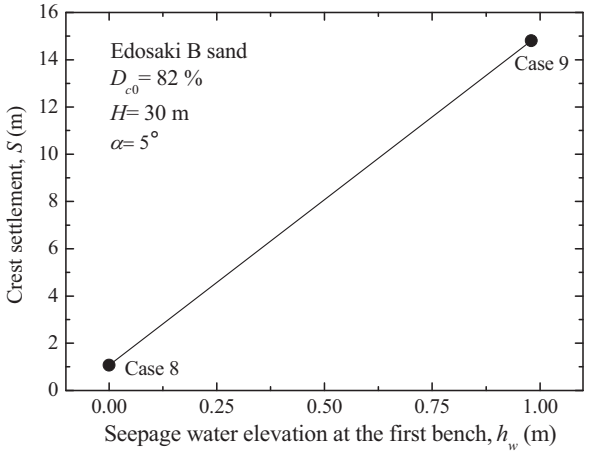

Fig. 17. Effects of seepage water elevation on crest settlement of embankments having a height of 30 m.

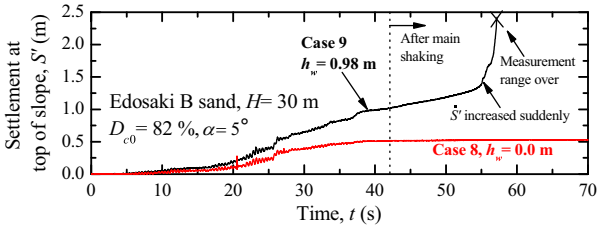

Fig. 18. Time history of settlement at top of slope of 30 m high embankments with different water tables.

base slope inclination on the seismic performance of embankments can also be seen in Fig. 21 when the data from cases 5 and 7 are compared.

In Fig. 21, the R_L value and the normalized maximum deviator stress, $q_{max}/2p'$, obtained from the triaxial test results shown in Figs. 6 and 4, respectively, are also plotted versus D_{c0}. The R_L and $q_{max}/2p'$ values of Edosaki sand increased with increasing D_{c0} as discussed previously. Fig. 22 shows S plotted versus R_L and $q_{max}/2p'$, where these data are derived from Fig. 21. The S value tended to decrease with increasing static and dynamic strengths of Edosaki sand, although it should be noted that the effects of the initial shear stress on the undrained behaviour were not taken into account in the triaxial tests for simplicity.

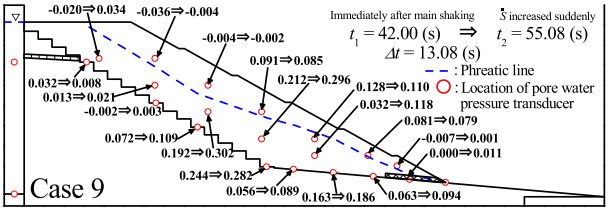

Fig. 19. Change in distribution of excess pore water pressure ratio after main shaking in case 9.

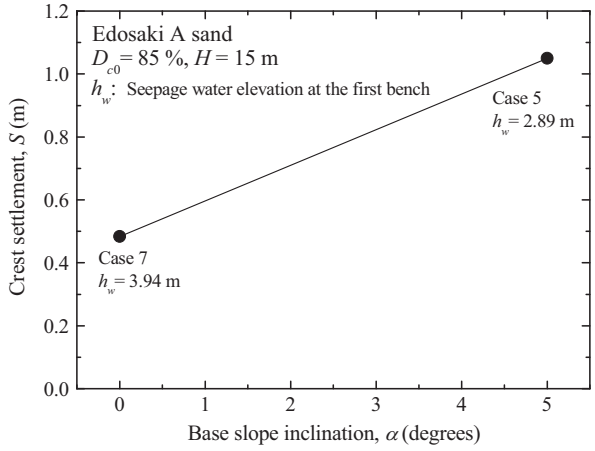

Fig. 20. Effects of base slope inclination on crest settlement.

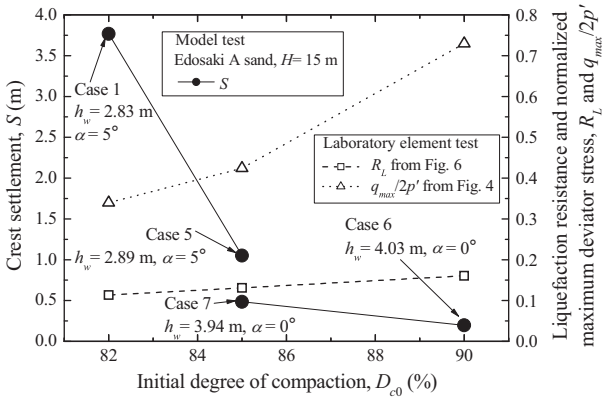

Fig. 21. Effects of soil density on crest settlement and strength properties of Edosaki sand.

Fig. 23 shows the time histories of A_{res} recorded by A3, R_u obtained by dividing Δu measured with P7 and P9 by the corresponding σ'_{v0}, and S associated with shaking. In the time trace of R_u, its maximum value, R_{umax}, and σ'_{v0} estimated by Eq. (3) are indicated as a reference. The following trends were observed from the figure.

1) The amplitude of A_{res} at each location tended to become smaller with decreasing D_{c0}, in particular in the positive direction, for every test. The possible reasons for this behaviour are: (a) the reduction in the shear modulus of embankments due to the accumulation of Δu, where the amount of Δu associated with shaking became large with decreasing D_{c0} as described below; and (b) earthquake-induced shear strain and associated distortion, where they became large with decreasing D_{c0} as shown in Fig. 9.
2) For every test, the value of S started to increase remarkably after A_{res} began to decay when compared with the input acceleration shown in Fig. 8(a) and after only a slight increase in R_u was attained. The delayed failure was observed in case 1 as mentioned previously, while the higher density prevented it from occurring due to the smaller R_u, showing that the occurrence of the time delay also depended on the embankment density.
3) The value of R_u increased from the very beginning of shaking. As typically shown in Fig. 23(f), some transducers showed that the R_u value tended to accumulate even after shaking and that both the total amount of R_u and the duration of its increase became large with decreasing D_{c0} and increasing α. The trend where larger D_{c0} resulted in the smaller earthquake-induced R_u was consistent with the laboratory test results shown in Fig. 4. However, complete liquefaction did not occur even in the loosest case, D_{c0}=82%, as discussed previously with regard to the test results shown in Fig. 14.

5.6. Effects of fill material

Fig. 24 shows the comparison between the test results on Edosaki B sand and Noto silt, where the F_c and U_c values of the

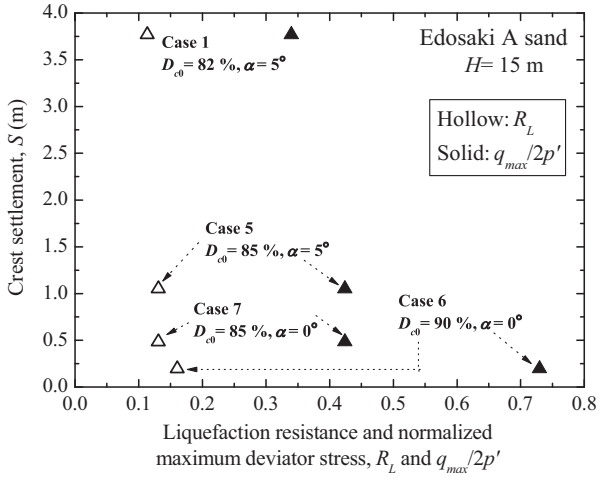

Fig. 22. Relationship between crest settlement and strength properties of Edosaki sand.

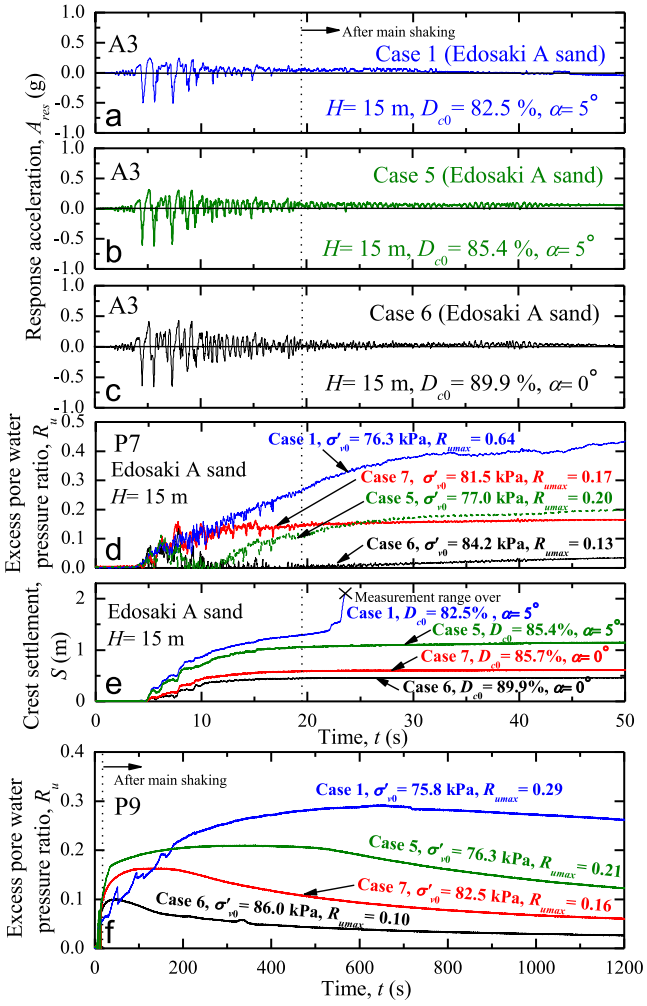

Fig. 23. Time history data of embankments consisting of Edosaki A sand with different densities: (a) through (c) response accelerations recorded by A3, (d) excess pore water pressure ratio from P7, (e) crest settlement, and (f) excess pore water pressure ratio from P9.

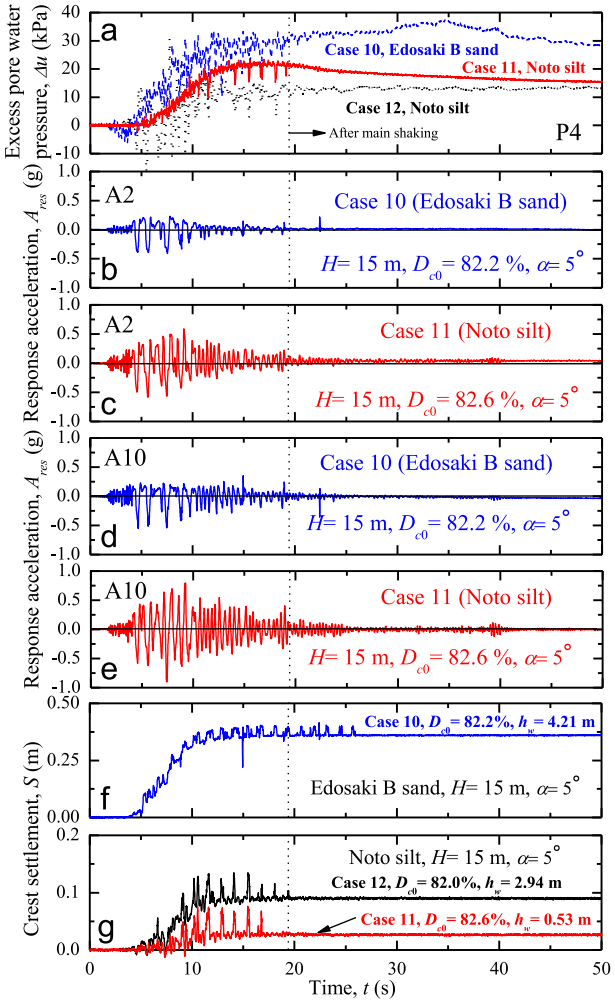

Fig. 24. Comparison between time history data of model tests on Edosaki B sand and Noto silt: (a) excess pore water pressure measured with P4, (b) through (e) response accelerations recorded by A2 and A10, and (f) and (g) crest settlement.

latter material were much larger than those of the former one as shown in Table 1 and Fig. 1(a). It may be seen from Fig. 9 that the seepage water elevations of cases 10 and 12 were similar. The following trends were observed from Fig. 24.

1) The Δu value of Noto silt was smaller than that of Edosaki B sand. This trend was consistent with the laboratory test results shown in Figs. 3 and 5. In addition, in cases 11 and 12, the accumulation of Δu stopped immediately after the main shaking, unlike case 10.
2) Correspondingly, the A_{res} value of Noto silt was larger than that of Edosaki B sand at both the lower and upper parts of embankments. This result suggests that the embankment consisting of Noto silt behaved more rigidly.
3) The S values of cases 11 and 12 were much smaller than that in case 10. In three cases (Fig. 24(f) and (g)), the values of S became almost constant immediately after the main shaking.

Fig. 25 shows the effects of the static and dynamic strength properties of both materials on the seismic performance of embankments, where the values of S for cases 10 through 12 discussed in Fig. 24 are plotted versus those of R_L and $q_{max}/2p'$ obtained from the triaxial test results shown in Figs. 6 and 3, respectively. It may be seen that larger R_L and $q_{max}/2p'$ tended to result in smaller S. Since the R_L and $q_{max}/2p'$ values of Noto silt were about 70% larger than those of Edosaki sand, the effects of the strength properties on the seismic behaviour may have been predominant even after taking the slight difference among the model phreatic lines into account.

As pointed out by Tatsuoka (2011), with increasing compaction energy, the ρ_{dmax} values of well-graded sandy soils containing a high percentage of fine particles tend to increase while those of poorly graded clean sands do not change significantly. This result suggests that properly compacting fill materials with a high percentage of fine particles requires larger compaction energy. As a consistent field observation result by Mori et al. (2012), the SPT N values of the fill materials that included a large amount of fine particles, which was severely damaged by the 2011 off the Pacific coast of Tohoku earthquake, ranged from 0 to 5 in most sites of Sendai city, suggesting that those fill materials tend to be poorly compacted during the construction works and, consequently, reflect the loose state of embankments. On the other hand,

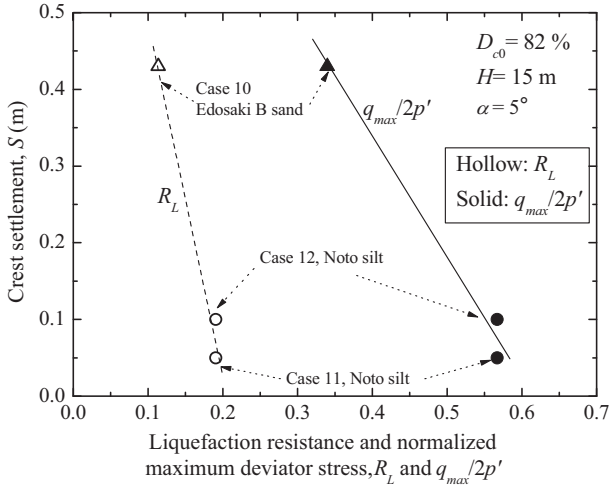

Fig. 25. Relationship between crest settlement and strength properties of Edosaki B sand and Noto silt.

the test results described in this section suggest that the seismic performance of embankments consisting of well-graded silty soils with large F_c values may be higher than that of poorly graded sands under otherwise the same conditions if field compaction works are performed properly. The effects of the grading characteristics of fill materials on the seismic performance of embankments have not been systematically studied and not well understood, so further studies on this issue should be carried out.

According to the survey results by Mori et al. (2012), the fill material with the large F_c value also led to the rise of the water tables in most cases due possibly to its large amount of fine particles and the poor performance of drainage systems. Due attention should be paid to the construction of adequate drainage systems as well as proper compaction works when those soils are used as fill materials.

6. Conclusions

The following conclusions can be derived from the test results described in this paper:

1. Seepage water was one of the causative factors of earthquake-induced embankment failure. The seismic performance of embankments was remarkably improved by lowering the seepage water elevation by means of the toe drain. In the construction of hillside embankments, the placement of appropriate drainage systems is very important to prevent earthquake-induced damage.
2. The deformation of loosely compacted embankments with a shallow water table proceeded progressively even after the main shaking has ceased and their crest settlements observed after the main shaking were larger than those developed during the main shaking, indicating delayed failure. Immediately after shaking, deformation was concentrated below the water table and near the embankment toe, while the delayed failure occurred near the water table. The delayed failure observed in the present study appears to have been attributed to the multiple effects of upward seepage associated with the redistribution of excess pore water pressures generated during the main shaking, continued small vibration after the main shaking, and driving static shear stresses caused by the embankment weight.
3. The seismic performance of large-scale embankments can be remarkably improved by installing toe drains.
4. Larger base slope inclination produced larger deformation of embankments due to the increase in the downslope driving force caused by the embankment weight.
5. Embankments can be designed to resist earthquake-induced damage by increasing the strength of fill materials by means of proper compaction. The higher embankment density prevented the occurrence of earthquake-induced delayed failure due to the smaller excess pore water pressure. On the other hand, with decreasing embankment density, the amplitude of the response acceleration tended to become smaller. Some transducers showed that the excess pore water pressure tended to accumulate even after the main shaking and that both the extent of the increase and the duration of the increase became larger with decreasing density and increasing slope inclination.
6. Fill materials with a high percentage of fine particles tend to lead to poor compaction during the construction works, suggesting that the proper compaction of those materials requires larger compaction energy. However, the model test results showed that if field compaction works were performed properly, the seismic performance of embankments consisting of well-graded silty soils with the large fines content was higher than that of poorly graded sands.

References

Amaya, M., Sato, T., Koseki, J., Maeshiro, N., 1997. Undrained cyclic shear characteristics of Toyoura sand under low confining stress. In: Proc. 52nd Annual Conf. Jpn. Soc. Civil Engineers, (vol. 3-A), pp. 130–131 (in Japanese).

Arab, A., Belkhatir, M., 2012. Fines content and cyclic preloading effect on liquefaction potential of silty sand: a laboratory study. Acta Polytech. Hung. 9 (4), 47–64.

Castro, G., 1969. Liquefaction of sands. Harvard Soil Mechanics Series, 81. Harvard University, Cambridge, MA.

Chien, L.-K., Oh, Y.-N., Chang, C.-H., 2002. Effects of fines content on liquefaction strength and dynamic settlement of reclaimed soil. Can. Geotech. J. 39, 254–265.

Creager, W.P., Justin, J.D., Hinds, J., 1945. Engineering for Dams, Earth, Rock-fill, Steel and Timber dams. John Wiley & Sons, Inc., NY 645–649 III.

Dobry, R., Taboada, V., Liu, L., 1997. Centrifuge modeling of liquefaction effects during earthquakes. In: Balkema, A.A. (Ed.), Proc. IS-TOKYO'95/ The First Intl. Conf. on E.q. Geotech. Engrg., November 14–16, 1995, Tokyo, pp. 1291–1324.

Egawa, T., Nishimoto, S., Tomisawa, K., 2004. An experimental study on the seismic behavior of embankments on peaty soft ground through centrifuge model tests. In: 13th World Conference on Earthquake Engineering, Paper no. 36.

Hamada, M., 1992a. Large ground deformations and their effects on lifelines: 1964 Niigata earthquake. Case Studies of Liquefaction and Lifeline Performance During Past Earthquakes, 1. Natl. Center for Earthquake Engineering Research, State Univ. of New York, Buffalo, NY.

Hamada, M., 1992b. Large ground deformations and their effects on lifelines: 1983 Nihonkai-Chubu earthquake. Case Studies of Liquefaction and Lifeline Performance During Past Earthquakes, 1. Natl. Center for Earthquake Engineering Research, State Univ. of New York, Buffalo, NY.

Higo, Y., Kimura, R., Kimoto, S., Oka, F., Doi, T., Lee, C.-W., Kinugawa, T., 2012. Dynamic centrifuge model tests on unsaturated road embankment with toe drain and their simulations. In: Proc. the 67th Annual Convention of JSCE, III-vol. 203–204 (in Japanese).

Hwang, D., Yanagisawa, E., Sugano, T., 1993. Shear characteristics of silt containing sand. III. J. Jpn. Soc. Civ. Eng. 22, 25–33 (in Japanese).

Hyodo, M., Hyde, A., Aramaki, N., Nakata, Y., 2002. Undrained monotonic and cyclic shear behavior of sand under low and high confining stresses. Soils Found. 42 (3), 63–76.

Ishihara, K., Koseki, J., 1989. Cyclic Shear Strength of Fines-containing Sands. Earthquake and Geotechnical Engineering, Japanese Society of Soil Mechanics and Foundation Engineering, pp. 101–106.

Japanese Society of Civil Engineers, 1966. The Report of Damage Investigation in the 1964 Niigata Earthquake. Japanese Society of Civil Engineers (JSCE), Tokyo (in Japanese).

Kanatani, M., Nishi, K., Tanaka, Y., 1994. Dynamic properties of sand at low confining pressure. In: Shibuya, Mitachi, Miura (Eds.), Pre-failure Deformation of Geomaterials, vol. 1. Balkema, pp. 37–40.

Kawakami, F., Asada, A., 1966. Damage to the ground and earth structures by the Niigata earthquake of June 16, 1964. Soils Found. 6 (1), 14–30.

Koseki, J., Sasaki, T., Wada, N., Hida, J., Endo, M., Tsutsumi, Y., 2006. Damage to earth structures for national highways by the 2004 Nigata-ken Chuetsu earthquake. Soils Found. 46 (6), 739–750.

Kutter, B.L., James, R.G., 1989. Dynamic centrifuge model tests on clay embankments. Geotechnique 39 (1), 91–106.

Law, K.T., Ling, Y.H., 1992. Liquefaction of granular soils with non-cohesive and cohesive fines. In: Proc. 10th World Conf. on Earthquake Engineering, Balkema, Rotterdam, Netherlands, pp. 1491–1496.

Matsuo, O., 1996. Damage to River Dikes. Soils and Foundations, Special issue 1 on Geotechnical Aspects of the January 17 1995, Hyogoken-Nambu Earthquake, pp. 235–240.

Matsuo, O., Tsutsumi, T., Kondoh, K., Tamoto, S., 1998. The dynamic geotechnical centrifuge at PWRI. In: Balkema, A.A. (Ed.), Proc. Intl. Conf. CENTRIFUGE'98, September 23–25, 1998, Tokyo, pp. 25–30.

Matsuo, O., Saito, Y., Sasaki, T., Kondoh, K., Sato, T., 2002. Earthquake-induced flow slides of fills and infinite slopes. Soils Found. 42 (1), 89–104.

Mochizuki, Y., Fukushima, S., 1993 Liquefaction characteristics of saturated sand at low pressure. In: Proc. 28th Jpn. Natl. Conf. SMFE, pp 917–918 (in Japanese).

Mori, T., Tobita, Y., Okimura, T., 2012. The damage to hillside embankments in Sendai city during the 2011 off the Pacific Coast of Tohoku Earthquake. Soils Found. 52 (5), 910–928.

Okamura, M., Abdoun, T.H., Dobry, R., Sharp, M.K., Taboada, V.M., 2001. Effects of sand permeability and weak aftershocks on earthquake-induced lateral spreading. Soils Found. 41 (6), 63–77.

Okamura, M., Tamamura, S., 2011. Seismic stability of embankment on soft soil deposit. Int. J. Phys. Modell. Geotech. 11 (2), 50–57.

Okimura, T., Futaki, M., Okamoto, A., Nanbu, M., 1999. Investigation of relationship between damages to housing lots by the Hyogoken-Nanbu earthquake and various factors. J. Constr. Manage. Eng. JSCE 623 (IV-43), 259–270 (in Japanese).

Park, S.-S., Kim, Y.-S., 2013. Liquefaction resistance of sands containing plastic fines with different plasticity. J. Geotech. Geoenviron. Eng. ASCE, 825–830.

Pilgrim, N.K., 1998. Earthquake-related deformation beneath gently inclined ground. Geotechnique 48 (2), 187–199.

Public Works Research Institute (PWRI), 1971. Survey on Disaster Caused by the Tokachi-oki Earthquake 1968. In: Report of PWRI, 141, pp. 67–77 (in Japanese).

Public Works Research Institute (PWRI), 2008. Report on Damage to Infrastructures and Buildings by the 2007 Noto-Hanto Earthquake. In: Report of PWRI, 4087, pp. 105–153 (in Japanese).

Sasaki, Y., Oshiki, H., Nishikawa, J., 1994. Embankment Failure Caused by the Kushiro-oki Earthquake of January 15, 1993. Performance of Ground and Soil Structures during Earthquakes, Special Volume for 13th ICSMGE, New Delhi, India, pp. 61–68.

Sasaki, Y., Towhata, I., Miyamoto, K., Shirato, M., Narita, A., Sasaki, T., Sako, S., 2012. Reconnaissance report on damage in and around river levees caused by the 2011 off the Pacific coast of Tohoku earthquake. Soils Found. 52 (5), 1016–1032.

Seed, H.B., 1979. Considerations in the earthquake resistant design of earth and rockfill dams. Geotechnique 29 (3), 214–263.

Sento, N., Kazama, M., Uzuoka, R., Ohmura, H., Ishimaru, M., 2004. Possibility of postliquefaction flow failure due to seepage. J. Geotech. Geoenviron. Eng. ASCE, 707–716.

Sitharam, T.G., Dash, H.K., Ravishankar, B.V., 2013. Postliquefaction undrained shear behavior of sand-silt mixtures at constant void ratio. Int. J. Geomech. ASCE 13 (4), 421–429.

Tatsuoka, F., 2011. Laboratory stress–strain tests for developments in geotechnical engineering research and practice. Bishop Lecture. In: Proc. of International Symposium on Deformation Characteristics of Geomaterials, September 1–3, 2011, Seoul, Korea.